

Investigation of the Incorporation of C₆₀ into PC₆₁BM to Enhance the Photovoltaic Performance of Inverted-type Perovskite Solar Cells Based on MAPbI₃

Mehmet Kazici^{1,*}

¹Department of Electrical & Electronics Engineering, Engineering Faculty, Siirt University, 56100, Siirt, TURKEY

<https://orcid.org/0000-0001-9048-7788>

*corresponding author: mehmetkazici@siirt.edu.tr

(Received: 27.10.2023, Accepted: 15.11.2023, Published: 23.11.2023)

Abstract: Perovskite Solar Cells (PSCs) have managed to significantly capture attention by achieving efficiency values of 25.6% in a remarkably short period of around ten years. Each layer within the device plays a crucial role in the overall device efficiency when it comes to PSC production. PC₆₁BM, a derivative of fullerene, is one of the most commonly used electron-transport layers (ETLs) in inverted-type PSCs. In this study, the improvement of the ETL was aimed by incorporating C₆₀ into PC₆₁BM, and the effects of the doped ETL on MAPbI₃-based inverted-type PSCs were investigated. For inverted type PSCs which are fabricated under high humidity (40-60%) and room conditions (~25 °C), the power conversion efficiencies (PCEs) have boosted from 11.54% (for undoped PC₆₁BM) to 13.40% (for C₆₀-doped PC₆₁BM). To comprehend the sources of improvement in the fabricated devices, a series of characterizations were carried out, including Current Density-Voltage (J-V), Hysteresis Factor (HF), Scanning Electron Microscope (SEM), and Atomic Force Microscope (AFM) measurements.

Key words: Perovskite solar cells, Fullerene, Electron transport layer

1. Introduction

Perovskite solar cells (PSCs) have achieved a remarkable increase in efficiency, from 3.8% to 25.6%, in a relatively short period of about a decade [1, 2]. PSCs have garnered significant attention from researchers worldwide due to their easy production, high efficiency, and cost-effectiveness. Perovskite materials typically have a chemical structure represented as ABX₃. In the desired semiconductor structure of halide perovskites for photovoltaic applications, ABX₃ consists of: A = cation (such as CH₃NH₃⁺ and CH(NH₂)₂⁺), B = divalent metal cation (such as Pb²⁺), and X = halogen anion (such as Cl⁻, Br⁻ and I⁻) [3]. In 2009, Miyasaka and their colleagues discovered that the organic metal halide perovskite materials, Methyl ammonium lead bromide (MAPbBr₃) and Methyl ammonium lead iodide (MAPbI₃), could absorb sunlight in dye-sensitized solar cells. They achieved an efficiency of 3.8% by using perovskite materials inside liquid electrolytes [1]. However, it was observed that perovskite materials degraded rapidly within liquid electrolytes, leading to research efforts to find more suitable production methods for perovskite. In 2012, using thin-film technology, the first all-solid-state PSCs were fabricated, and device stability was improved, reaching efficiency values of 9.7% [4]. In the same year, Snaith and their colleagues used compact titanium dioxide (TiO₂) as the electron transport layer (ETL) and aluminum oxide (Al₂O₃) as the scaffold material, achieving an efficiency of 10.9% for PSCs by using the perovskite material methyl ammonium lead iodide chloride (CH₃NH₃PbI₂Cl) [5]. Recently, all-solid-state single

junction PSCs have reached efficiency values of 25.6% [2]. Thin-film layers involved in every stage of fabrication for PSCs are crucial in terms of production cost, stability, and efficiency. In traditional and inverted device architectures of PSCs, the main aim is to transport the charges generated in the absorber layer (perovskite) to the necessary electrodes through charge transport layers. Therefore, charge transport layers play a significant role in the device efficiency. The orientation of the electron-hole (exciton) pairs formed in the absorber layer is the most fundamental difference between traditional and inverted type PSCs. In the traditional architecture, electrons move towards the bottom electrode, whereas in the inverted architecture, they move towards the top electrode. Similarly, in the traditional device architecture, holes move towards the top electrode, while in the inverted structure, holes move towards the bottom electrode. In the PSCs fabricated using traditional device architecture, inorganic oxide materials such as titanium dioxide (TiO₂) [4, 5, 6] and tin (IV) oxide (SnO₂) [7, 8] are commonly used as ETLs. On the other hand, in the inverted device architecture, ETLs often involve fullerene and its derivatives, known for their ultrafast charge transfer properties [9, 10]. The inverted device architecture has gained attention for commercial applications due to its low-temperature production techniques and ease of manufacturability [11]. Phenyl-C₆₁-butyric acid methyl ester (PC₆₁BM), a derivative of fullerene, is one of the most commonly used electron transport materials in the inverted type PSCs due to its strong electron transport capabilities and relatively high electron affinity [12]. However, PC₆₁BM can lead to efficiency reduces in the inverted type PSCs due to certain limitations, including low electron mobility, challenges in forming high-quality thin films, current leakage, and excessive nonradiative recombination [10, 13]. To overcome the disadvantages mentioned above, one of the most effective methods is to apply a doping process into PC₆₁BM. Kuang and their colleagues enhanced device performance in CH₃NH₃PbI_{3-x}Cl_x-based PSCs by introducing a new two-dimensional carbon material called graphdiyne as a dopant into PC₆₁BM. This approach enhanced film conductivity and improved the electron transport layer/perovskite interface [14]. Bae and their colleagues boosted the PCE of PSCs by employing n-type 1,3-Dimethyl-2-phenyl-2,3-dihydro-1H-benzimidazole (DMBI) as a dopant into PC₆₁BM. This addition increased the electrical conductivity of the ETL while reducing the work function [15]. Xia and their colleagues enhanced device efficiency by incorporating Oleamide, an amphiphilic surfactant, into PC₆₁BM. This modification improved the coverage of ETL on the perovskite surface, increased the flow of the charge to the top electrode, and significantly reduced recombination [16]. Similar doping strategies with PC₆₁BM, such as reduced graphene oxide (RGO) [17], carbon quantum dots [18], bathocuproine (BCP) [19] and poly[(9,9-dioctylfluorene)-2,7-diyl-alt-(4,7-bis(3-hexylthien-5-yl)-2,1,3 benzothiadiazole)-2',2''-diyl] (F8TBT) [20], have been utilized to enhance the PCEs of PSCs. In 2021, Younes and their colleagues improved device performance and stability for inverted type PSCs by directly doping fullerene (C₆₀) into PC₆₁BM, serving as an ETL [21]. In this study, chlorobenzene was used as a solvent for both PC₆₁BM and C₆₀ materials, and the research investigated very low concentration ratios of C₆₀ within PC₆₁BM. The device fabrication involved preparing perovskite (MAPbI₃) in dimethyl sulfoxide (DMSO) and gamma-butyrolactone (γ -butyrolactone) solvents, and perovskite and ETLs were deposited in a glove box with low oxygen and humidity conditions. However, it's important to note that commercializing PSCs with device fabrication inside a glove box can be both challenging and costly.

In this present study, PSCs based on MAPbI₃ were fabricated using gamma-butyrolactone as a solvent under high humidity conditions (40-60%) and room temperature (~25 °C) for the inverted architecture. The aim was to improve device efficiency by incorporating C₆₀ into PC₆₁BM as the electron transport layer. Unlike previous studies, 1,2-dichlorobenzene, which is a good solvent for C₆₀, was specifically used for the electron

transport layer, and the amount of PC₆₁BM was reduced, with C₆₀ being added in its place. The efficiency of the fabricated PSCs increased from 11.54% (for undoped PC₆₁BM) to 13.40% (for C₆₀-doped PC₆₁BM), as compared to the reference device.

2. Material and Method

2.1. Device Fabrication

The inverted type PSCs were fabricated with the ITO/PEDOT:PSS/MAPbI₃/PC₆₁BM or PC₆₁BM:C₆₀/BCP/Ag device architecture. Indium tin oxide (ITO)-coated glass substrates (Japan, 10-12 ohm/square resistance) were first cleaned by sonication in acetone and isopropanol for 20 minutes each and then dried with nitrogen gas. Before the spin-coating process, the cleaned ITO-coated glass substrates were exposed to oxygen plasma for 10 minutes (Germany, Diener-Femto). As the hole transport layer, PEDOT:PSS (Heraeus, AL4083) was coated onto the ITO-coated glass using the spin-coating method. After the deposition of PEDOT:PSS thin films, a 10-minute annealing process was carried out at 140 °C. The perovskite solution was prepared by mixing PbI₂ (Sigma Aldrich, 1.3 M) and CH₃NH₃I (Lumtec, 1.54 M) materials in 2.5 mL of gamma-butyrolactone (GBL) and stirring on a magnetic stirrer at 50 °C for 24 hours. Prior to coating, the perovskite solution was filtered using a 0.45 μm PTFE filter. Subsequently, the perovskite solution was spin-coated onto the PEDOT:PSS layer at 5000 rpm for 40 seconds. During the last 10 seconds of the spin-coating process, a washing step with 80 μL of toluene was applied as an anti-solvent while coating the perovskite onto the PEDOT:PSS layer. The perovskite films were annealed at 100 °C for 20 minutes. PC₆₁BM (Lumtec) (20 mg) and PC₆₁BM:C₆₀ (18 mg:2 mg) were separately prepared in 1 mL of 1,2-dichlorobenzene solvent and mixed on a magnetic stirrer for 12 hours without temperature application. The PC₆₁BM and PC₆₁BM:C₆₀ solutions were then spin-coated onto the perovskite surface at 2000 rpm for 35 seconds. The BCP (Lumtec) solution (0.5 mg/mL in ethanol) was spin-coated on ETL at 4000 rpm for 45 seconds. Finally, a 110 nm-thick silver (Ag) top metal electrode was deposited using thermal evaporation method. Throughout the device fabrication process, all steps except for the top metal electrode deposition were carried out under ambient conditions with high humidity levels (40-60%).

PCEs and hysteresis factor (HF) of fabricated devices were calculated by using the following equations:

$$PCE(\%) = \left(\frac{P_{out}}{P_{in}} \right) \times 100 = \frac{J_{sc} \times V_{oc} \times FF}{P_{in}} \times 100 \quad (1)$$

$$HF(\%) = \frac{|PCE_{Forward} - PCE_{Reverse}|}{PCE_{Forward}} \times 100 \quad (2)$$

3. Results

Fullerene and its derivatives are among the most often utilized ETLs for inverted-type (IT) PSCs. The effects of using of fullerene (C₆₀) in its derivative (PC₆₁BM) as ETLs for PSCs have been investigated on device performance. IT-PSCs were fabricated with the device configuration of ITO/PEDOT:PSS/MAPbI₃/PC₆₁BM or PC₆₁BM:C₆₀/BCP/Ag. The fabricated device architecture and molecular structures of C₆₀ and PC₆₁BM were illustrated in figure 1.

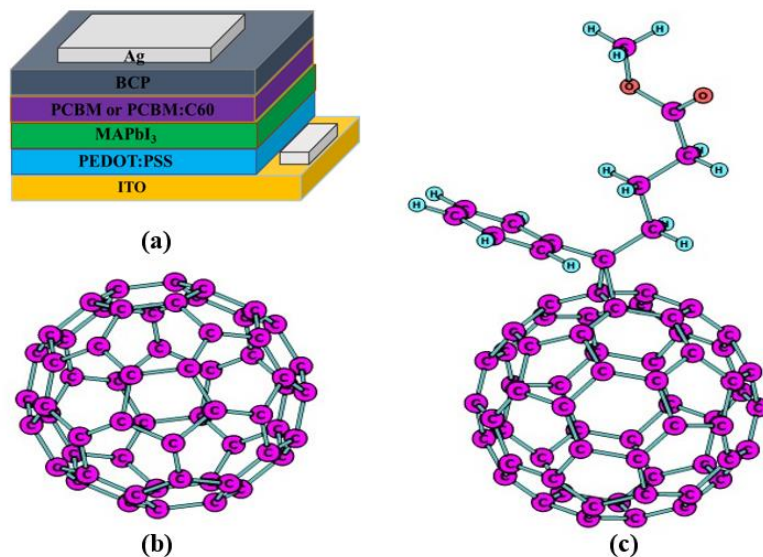


Figure 1. (a) Device structure of inverted-type PSC and molecular structures of (b) C_{60} and (c) $PC_{61}BM$

In order to determine the photovoltaic parameters of the fabricated IT-PSCs, current density-voltage (J - V) measurements were carried out. The photocurrent density-voltage (J - V) characteristics were measured under AM 1.5G irradiation at 100 mW/cm^2 . Figure 2 displays J - V curves of control ($PC_{61}BM$ as ETL) and champion ($PC_{61}BM:C_{60}$ as ETL) devices. In the absence of any small amounts of C_{60} additives, utilizing pristine $PC_{61}BM$ as the ETL (control device), the cell exhibited a short-circuit current density (J_{SC}) of 16.92 mA/cm^2 , an open circuit voltage (V_{OC}) of 1015 mV and a fill factor (FF) of 67.2% . The photovoltaic parameters resulted in a power conversion efficiency (PCE) of 11.54% for the control device, with an average PCE of 10.37% across the fifteen fabricated devices. The addition of the C_{60} into $PC_{61}BM$ (champion device) boosted PCE to 13.40% with a J_{SC} of 18.36 mA/cm^2 , a V_{OC} of 986 mV and a FF of 74.0% (average PCE of 12.91% for fifteen devices).

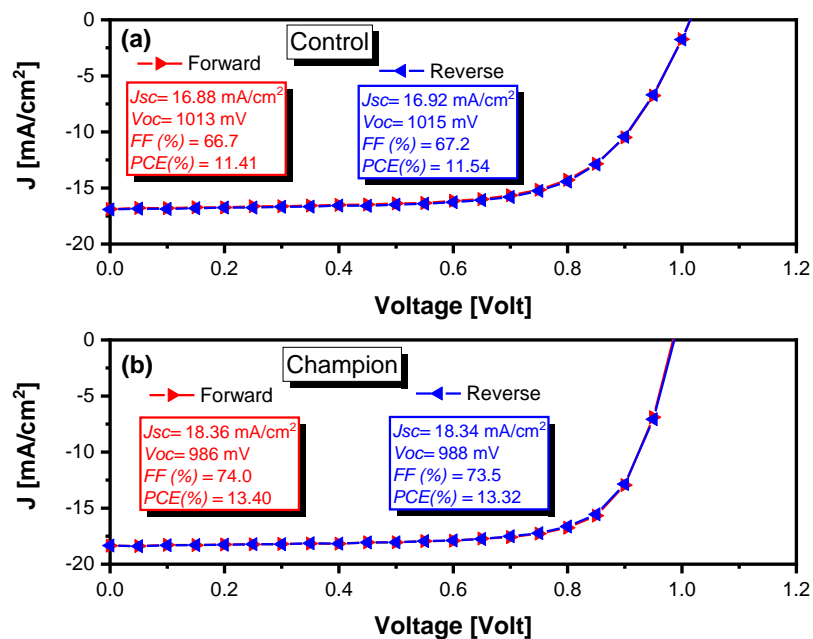


Figure 2. Current density (J) - Voltage (V) curves for (a) control and (b) champion devices

When the best efficiency values for the control and champion devices are compared, it is found that using C_{60} as the additive in ETL improves the PCE by approximately 16% . The primary factors contributing to this enhancement are clearly discernible in the form

of increased J_{SC} and FF . It is evident that the addition of C_{60} into $PC_{61}BM$ has significantly boosted J_{SC} , increasing it from 16.92 mA/cm^2 (control) to 18.36 mA/cm^2 (champion), and FF has also improved from 67.2% to 74.0% . Another factor that affects the $PCEs$ of PSCs is the current-voltage hysteresis. To comprehend the hysteresis effect of C_{60} as an additive in $PC_{61}BM$ on PSCs, both forward and reverse scans were carried out during $J-V$ measurements. Photovoltaic parameters and HF values for control and modified devices are provided in Table 1. Table 1 reveals that the hysteresis factors for the control and champion devices were computed as 1.14% and 0.60% , respectively. It can be said that the negligible level of hysteresis factor obtained for the champion device might lead to improvements in the charge carrier extraction when C_{60} is added into $PC_{61}BM$. The average $PCEs$ were determined based on a total of 30 distinct fabricated devices.

Table 1. Photovoltaic parameters of fabricated devices

ETL		J_{SC} (mA/cm^2)	V_{OC} (mV)	FF (%)	PCE (%)		HF (%)
					Best	Average	
$PC_{61}BM$ (Control)	Forward	16.88	1013	66.7	11.41	10.37	1.14
	Reverse	16.92	1015	67.2	11.54		
$PC_{61}BM:C_{60}$ (Champion)	Forward	18.36	986	74.0	13.40	12.91	0.60
	Reverse	18.34	988	73.5	13.32		

The surface morphology of the layers within PSCs has a substantial impact on their photovoltaic performance. Therefore, in order to gain a better understanding of the impact of C_{60} on the photovoltaic parameters, Scanning Electron Microscope (SEM) measurements were conducted. SEM images of $PC_{61}BM$ and $PC_{61}BM:C_{60}$ layers on the perovskite were depicted in Figure 3.

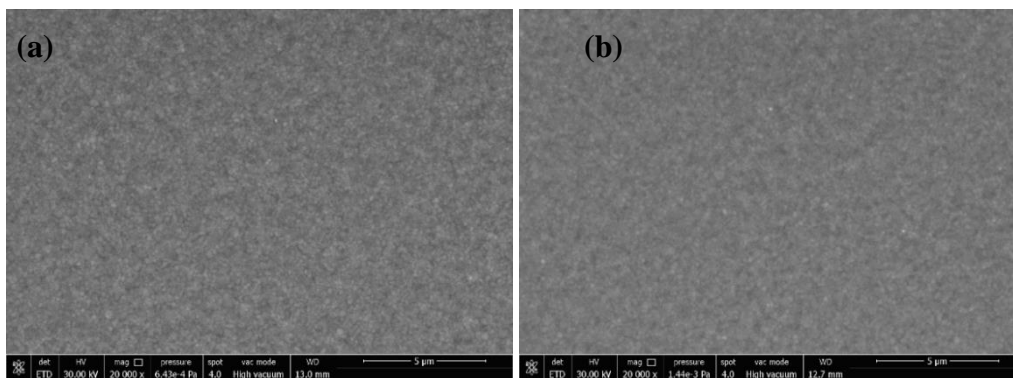


Figure 3. SEM images for (a) $PC_{61}BM$ and (b) $PC_{61}BM:C_{60}$ layers on perovskite

It was realized that the ETLs deposited on perovskite appear to be quite uniform based on SEM measurements. There are almost no pinholes observed in films coated with both $PC_{61}BM$ and $PC_{61}BM:C_{60}$ on perovskite. To delve deeper into the effects of incorporating C_{60} into the ETL surface, atomic force microscopy (AFM) measurements were performed. In this way, it could be gained a more detailed understanding of the morphology of both the perovskite/ $PC_{61}BM$ and the perovskite/ $PC_{61}BM:C_{60}$ surfaces. 2D and 3D AFM images of $PC_{61}BM$ and $PC_{61}BM:C_{60}$ surfaces deposited on perovskite layers were illustrated in Figure 4. The Root mean square (RMS) roughness values for the interfaces of perovskite/ $PC_{61}BM$, perovskite/ $PC_{61}BM:C_{60}$ are 5.20 nm and 4.50 nm , respectively. It is evident that the $PC_{61}BM:C_{60}$ surface is smoother than the $PC_{61}BM$ surface from the AFM images. Thus, the incorporation of C_{60} into $PC_{61}BM$ enhanced the morphology of the ETL films, leading to smoother surfaces.

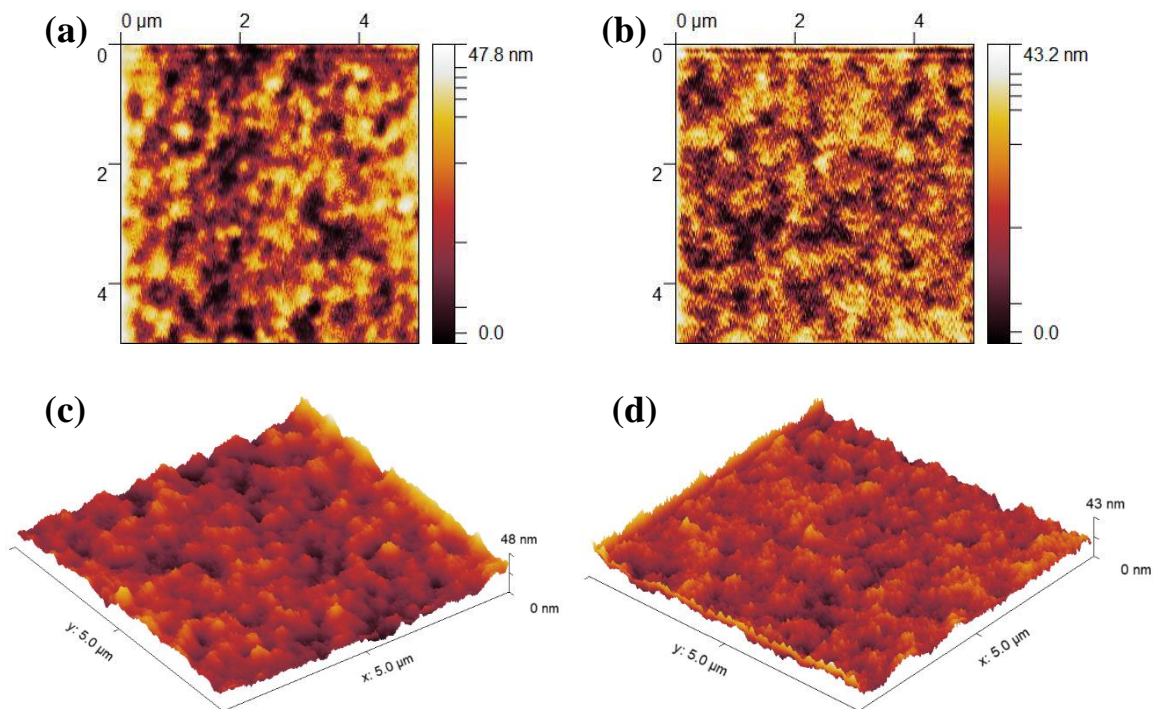


Figure 4. (a) 2D and (c) 3D AFM images of the PC₆₁BM surface on perovskite, and (b) 2D and (d) 3D AFM images of the PC₆₁BM:C₆₀ surface on perovskite

The smoother coated of the ETL on perovskite can prevent direct contact between the perovskite and the metal layer applied on ETL. Consequently, this situation might allow for more efficient charge transport between the metal contact and the ETL, leading to reduced charge recombination [21]. It can be concluded that the photovoltaic results obtained for both control and champion devices clearly demonstrate the considerable influence of this enhancement at the perovskite/ETL interface. In this study, a total of 30 different devices were fabricated with 15 serving as controls (PC₆₁BM used as ETL) and 15 incorporating C₆₀-doped ETLs, to investigate the impact of C₆₀ on photovoltaic performance. The statistical distribution of photovoltaic parameters for the fabricated devices is illustrated in Figure 5.

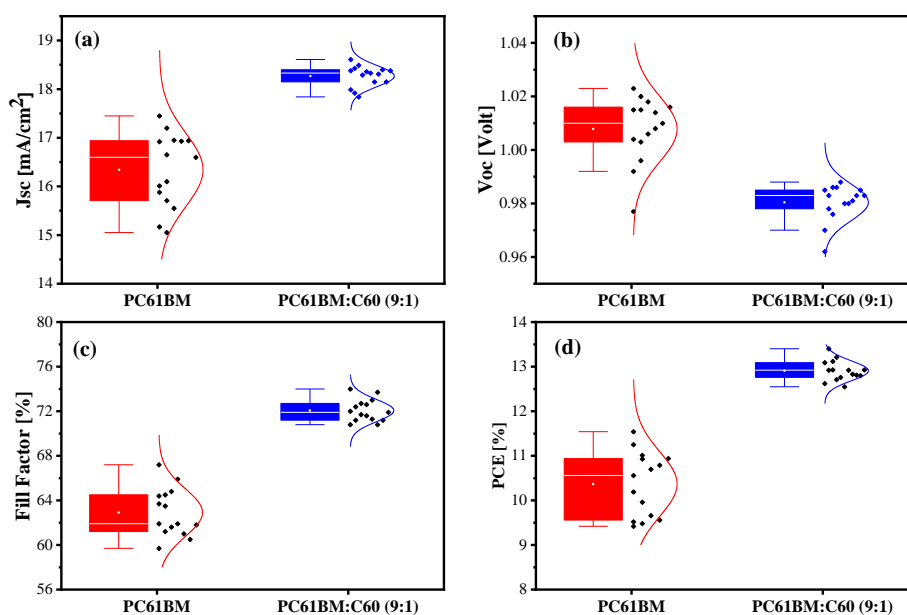


Figure 5. Statistic distribution of photovoltaic parameters for PSCs utilized PC₆₁BM and PC₆₁BM:C₆₀ as ETLs: distribution of (a) J_{SC} , (b) V_{OC} , (c) FF and (d) PCE .

In devices where pristine PC₆₁BM is used as the ETL, J_{SC} values are observed in the range of 15.05 to 17.45 mA/cm², while in devices where C₆₀-doped ETLs are employed, J_{SC} values have been observed in the range of 17.84 to 18.61 mA/cm². The minimum J_{SC} value (17.84) for C₆₀-doped devices surpasses the maximum J_{SC} value (17.45) for the reference device. V_{OC} values for devices with pristine ETLs range from 0.98 to 1.02 volt, whereas for doped ETLs, they range from 0.96 to 0.99 volt. There has been not a noticeable shift in V_{OC} . The FF values for control devices range from 59.7% to 67.2%, while for C₆₀-doped devices, they range from 70.8% to 74.0%. It is clear that there is a significant improvement in FF s as well. As a result, the enhancement of both J_{SC} and FF contributed to the increased PCE in devices incorporating C₆₀ into the ETL.

4. Conclusion

In this study, IT-PSCs were fabricated using MAPbI₃ perovskite structure under high humidity (40-60%) and room temperature (~25 °C) and C₆₀ was incorporated into PC₆₁BM as the ETL to improve PCEs of PSCs. The photovoltaic results demonstrated that by incorporating C₆₀ into the ETL, the PCE values for IT-PSCs were boosted from 11.54% to 13.40%. Additionally, it has been observed that the hysteresis factor decreased in devices with C₆₀ doping. SEM and AFM measurements were conducted to assess the impact of C₆₀ on the film morphology in PSCs. AFM images reveal that surface of C₆₀-doped ETL is smoother than the pristine ETL. The smoother surface of ETLs doped with C₆₀ is thought to avoid direct interaction between the metal contact on the ETL and the perovskite structure. As a result, devices with doped ETLs show significant improvements in J_{SC} and FF parameters, attributed to enhanced charge transport and reduced charge recombination.

Authorship contribution statement

M. Kazici: Investigation, Conceptualization, Methodology, Formal Analysis, Original Draft Writing, Review and Editing

Declaration of competing interest

The author declare that he has no known competing financial interests or personal relationships that could have appeared to influence the work reported in this paper.

Acknowledgment

I would like to express my gratitude to Prof. Dr. Mahmut Kus from the Department of Chemical Engineering at Konya Technical University for his contributions in providing me with laboratory facilities.

Ethics Committee Approval and/or Informed Consent Information

As the author of this study, I declare that I do not have any ethics committee approval and/or informed consent statement.

References

- [1] A. Kojima, K. Teshima, Y. Shirai and T. Miyasaka, "Organometal halide perovskites as visible-light sensitizers for photovoltaic cells", *Journal of the American Chemical Society*, 131, 6050–6051, 2009.
- [2] J. Jeong, M. Kim, J. Seo, H. Lu, P. Ahlawat, A. Mishra, Y. Yang, M. A. Hope, F. T. Eickemeyer, M. Kim, Y. J. Yoon, I. W. Choi, B. P. Darwich, S. J. Choi, Y. Jo, J. H. Lee, B. Walker, S. M. Zakeeruddin, L. Emsley, U. Rothlisberger, A. Hagfeldt, D. S. Kim, M. Grätzel and J. Y. Kim, "Pseudo-halide anion engineering for α -FAPbI₃ perovskite solar cells", *Nature*, 592, 381–385, 2021.

- [3] A. K. Jena, A. Kulkarni and T. Miyasaka, “Halide perovskite photovoltaics: background, status, and future prospects”, *Chemical Reviews*, 119, 3036–3103, 2019.
- [4] H. S. Kim, C. R. Lee, J. H. Im, K. B. Lee, T. Moehl, A. Marchioro, S. J. Moon, R. Humphry-Baker, J. H. Yum, J. E. Moser, M. Grätzel and N. G. Park, “Lead iodide perovskite sensitized all-solid-state submicron thin film mesoscopic solar cell with efficiency exceeding 9%”, *Scientific Reports*, 2, 591, 2012.
- [5] M. M. Lee, J. Teuscher, T. Miyasaka, T. N. Murakami and H. J. Snaith, “Efficient hybrid solar cells based on meso-superstructured organometal halide perovskites”, *Science*, 338, 643–647, 2012.
- [6] W. Hu, S. Yang and S. Yang, “Surface modification of TiO₂ for perovskite solar cells”, *Trends in Chemistry*, 2, 148–162, 2020.
- [7] W. Ke, G. Fang, Q. Liu, L. Xiong, P. Qin, H. Tao, J. Wang, H. Lei, B. Li, J. Wan, G. Yang and Y. Yan, “Lower temperature solution-processed tin oxide as an alternative electron transporting layer for efficient perovskite solar cells”, *Journal of the American Chemical Society*, 137, 6730–6733, 2015.
- [8] Q. Jiang, X. Zhang and J. You, “SnO₂: a wonderful electron transport layer for perovskite solar cells”, *Small*, 14, 1–14, 2018.
- [9] N. S. Sariciftci, L. Smilowitz, A. J. Heeger and F. Wudl, “Photoinduced electron transfer from a conducting polymer to buckminsterfullerene”, *Science*, 258, 1474–1476, 1992.
- [10] R. Zahran and Z. Hawash, “Fullerene-based inverted perovskite solar cell: a key to achieve promising, stable, and efficient photovoltaics”, *Advanced Materials Interfaces*, 9, 1–18, 2022.
- [11] X. Lin, D. Cui, X. Luo, C. Zhang, Q. Han, Y. Wang and L. Han, “Efficiency progress of inverted perovskite solar cells”, *Energy & Environmental Science*, 13, 3823–3847, 2020.
- [12] M. A. Kumari, T. Swetha and S. P. Singh, “Fullerene derivatives: a review on perovskite solar cells”, *Materials Express*, 8, 389–406, 2018.
- [13] D. Yang, X. Zhang, K. Wang, C. Wu, R. Yang, Y. Hou, Y. Jiang, S. Liu and S. Priya, “Stable efficiency exceeding 20.6% for inverted perovskite solar cells through polymer-optimized PCBM electron-transport layers”, *Nano Letters*, 19, 3313–3320, 2019.
- [14] C. Kuang, G. Tang, T. Jiu, H. Yang, H. Liu, B. Li, W. Luo, X. Li, W. Zhang, F. Lu, J. Fang and Y. Li, “Highly efficient electron transport obtained by doping PCBM with graphdiyne in planar-heterojunction perovskite solar cells”, *Nano Letters*, 15, 2756–2762, 2015.
- [15] J. H. Bae, Y. J. Noh, M. Kang, D. Y. Kim, H. B. Kim, S. H. Oh, J. M. Yun and S. I. Na, “Enhanced performance of perovskite solar cells with solution-processed n-doping of the PCBM interlayer”, *RSC Advances*, 6, 64962–64966, 2016.
- [16] F. Xia, Q. Wu, P. Zhou, Y. Li, X. Chen, Q. Liu, J. Zhu, S. Dai, Y. Lu and S. Yang, “Efficiency enhancement of inverted structure perovskite solar cells via oleamide doping of PCBM electron transport layer”, *ACS Applied Materials & Interfaces*, 7, 13659–13665, 2015.
- [17] J. S. Yeo, R. Kang, S. Lee, Y. J. Jeon, N. S. Myoung, C. L. Lee, D. Y. Kim, J. M. Yun, Y. H. Seo, S. S. Kim and S. I. Na, “Highly efficient and stable planar perovskite solar cells with reduced graphene oxide nanosheets as electrode interlayer”, *Nano Energy*, 12, 96–104, 2015.
- [18] X. Zhu, J. Sun, S. Yuan, N. Li, Z. Qiu, J. Jia, Y. Liu, J. Dong, P. Lv and B. Cao, “Efficient and stable planar perovskite solar cells with carbon quantum dots-doped PCBM electron transport layer”, *New Journal of Chemistry*, 43, 7130–7135, 2019.
- [19] Y. Wang, S. Dong, Y. Miao, D. Li, W. Qin, H. Cao, L. Yang, L. Li and S. Yin, “BCP as additive for solution-processed PCBM electron transport layer in efficient planar heterojunction perovskite solar cells”, *IEEE Journal of Photovoltaics*, 7, 550–557, 2017.
- [20] Y. Bai, H. Yu, Z. Zhu, K. Jiang, T. Zhang, N. Zhao, S. Yang and H. Yan, “High performance inverted structure perovskite solar cells based on a PCBM:polystyrene blend electron transport layer”, *Journal of Materials Chemistry A*, 3, 9098–9102, 2015.
- [21] E. M. Younes, A. Gurung, B. Bahrami, E.M. El-Maghraby and Q. Qiao, “Enhancing efficiency and stability of inverted structure perovskite solar cells with fullerene C₆₀ doped PC₆₁BM electron transport layer”, *Carbon*, 180, 226–236, 2021.